Surface plasmon polaritons in generalized slab heterostructures with negative permittivity and permeability

Kosmas L. Tsakmakidis, Christian Hermann, Andreas Klaedtke, Cécile Jamois, and Ortwin Hess

Advanced Technology Institute, School of Electronics and Physical Sciences, University of Surrey, Guildford, GU2 7XH, United Kingdom

We present a detailed analytical study of surface plasmon polaritons (SPPs) in generalized asymmetric slab waveguides with a core of negative permittivity and permeability. Profiting from the duality principle, we confine ourselves to the analysis of *p*-polarized (TM) SPP eigenmodes, which also occur in thin metallic films. It is shown that the left-handed (LH) structures considered here support a richer variety of SPPs when compared to their metallic counterparts. Depending on the refractive index distribution, the permittivity of each medium and the thickness of the core, a total of 30 solutions to the involved characteristic equation are identified in a unified manner and classified systematically. In order to identify conclusively all SPPs, we follow an analytical methodology based directly on the solution constraints inherent in the associated transcendental equation. This treatment reveals striking features of the formed SPP eigenmodes, such as the existence of "supermodes" when no SPP is supported at one of the slab interfaces. Moreover, our study reveals the opening of gaps in the SPP dispersion diagrams, occurrence of monomodal propagation for specific choices of the material parameters, presence of SPPs with no cutoff thickness and coexistence of three eigenmodes, with double mode-degeneracy points occurring twice. The eigenmodes with negative energy flux that give rise to negative group velocity are identified via a closed-form expression for the time-averaged power flow P in the guide. For each eigenmode, we examine the variation of P with the reduced slab thickness and discuss key features of the effective index geometric dispersion diagram, most of which are unique to the generalized structures studied herein.

I. INTRODUCTION

Structures exhibiting negative permittivity and permeability were first analyzed around 40 years ago by Veselago.[1] He coined for their description the term "left-handed (LH) materials" to stress that the electric field **E**, the magnetic field **H**, and the wave vector **k** of a monochromatic plane wave inside such materials form a left-handed triplet. Veselago hypothesized that a material of this kind could exist without contradicting any of the fundamental laws of physics and he showed that it would posses striking electromagnetic properties, such as inverse Doppler shift, antiparallel phase and group velocities, backward power flow, and negative refraction. Critical issues, such as the actual occurrence of negative refraction[2] and the possibility to enhance the evanescent waves,[3,4] have been elucidated lately in a series of theoretical,[5] numerical,[6] and experimental[7] investigations.

How to construct these metamaterials was not known until recently due to the absence of naturally occurring or artificial materials with negative magnetic permeability. Practical suggestions of how LH media could be realized experimentally were first given in a series of works by Pendry *et al.*,[8] who also predicted theoretically that these media could be used for the creation of a "perfect lens." After these insights, the physical construction of a composite LH structure has been demonstrated by Shelby *et al.*,[9] and the possibility of achieving subwavelength resolution of an object with the same structures has been shown with further experiments.[10]

The perfect-lens action mentioned before relies critically on the amplification of an object's near field in a surface wave (SW)-like manner inside a LH slab. Due to momentum mismatch, radiative waves cannot couple directly to the formed SWs (or surface polaritons) at the interfaces of the slab with positive-index media. Pendry, however, showed that the near field of an object, which describes its finest features and decays exponentially away form the source (evanescent), can couple to an exponentially increasing field inside the LH slab that decays similarly on the other side. The whole field pattern resembles that of a surface polariton, although the proof of its existence for the particular symmetrical structure considered by Pendry was not given in Ref. 3, as well as in other more detailed analyses.[11]

Generalizations of these studies were investigations of asymmetric LH slab configurations for lensing,[12] sensing and directional coupling[13] applications. In both cases, the role of the coupled surface polaritons at the two interfaces of the slab waveguide was shown to be of crucial importance. For the first class of applications, the asymmetry helped to improve the limit imposed on the image resolution by the losses of the core. For the second class it improved the amplification of the evanescent waves in the device-working region, leading to enhanced performance.

It is the purpose of this paper to identify and classify all surface plasmon[14] polariton (SPP) eigenmodes supported by generalized asymmetric slab heterostructures. To this end, a rigorous analytical study is pursued that proves that a total of 30 solutions to the involved characteristic equation giving the SPP eigenmodes can exist for all choices of the refractive index distribution, constitutive parameters ε and μ, and the thickness of the core. Such an approach is essential,[15] particularly for the investigation of asymmetric slab configura-

tions, because the graphical methodologies that have been proposed in the past for the modal analysis of LH waveguides[12] did not reveal all SPP eigenmodes. A suitably modified form of the associated transcendental equation, derived from macroscopic electrodynamics using the well-known boundary conditions for the tangential electric and magnetic-field components, obviates this limitation and allows an analytical, unified treatment. We will confine ourselves to the discussion of the geometric dispersion (SPP effective index versus reduced slab thickness) since negative material parameters occur near resonances; hence, all experimental realizations of LH materials considered thus far were for narrowbands. In addition, all transmission (lensing) analyses of LH slab heterostructures, as well as investigations of asymmetric LH (Ref. 13) and metallic[15,16] films in the past, involved mainly monochromatic waves. All the important modal features, such as the number and classification of modes, number and kind of cutoffs, field enhancement, phase reversal, and possible double mode-degeneracy occurrence, can be derived in a clear and conclusive way following this methodology.

The organization of the paper is the following. Section II will make some introductory remarks regarding SPP waves at a single interface between a right-handed (RH) and a LH material. Emphasis is given on the conditions for the existence of such waves, as these are used later when the effects of retardation are taken into account. Section III is devoted to the discussion of the SPP eigenmodes supported by an asymmetric slab waveguide with a negative refractive index core. Following a macroscopic analysis, the LH waveguide is treated as a boundary value problem. Special solutions of the scalar wave equation are sought, subject to boundary conditions, to obtain the characteristic equation of the SPP eigenmodes. From the restrictions inherent in this equation, which depend on the refractive index distribution, we identify all supported SPP eigenmodes and classify them as forward or backward propagating via a closed-form expression for the total power flow P in the guide. Finally, Sec. IV summarizes the paper presenting the main conclusions of the present study.

II. SURFACE PLASMON POLARITONS AT A PLANE LH/RH INTERFACE

The negative permittivity and permeability of a left-handed medium (LHM) allows the existence of surface waves (SWs), also called surface polaritons (SPs), at the interface with a right-handed medium (RHM).[17] In order to investigate these solutions and derive the conditions for their existence, we consider the geometry illustrated in Fig. 1. Here both media are considered to be semi-infinite, homogeneous[11] and isotropic.[18] Medium 1 has negative relative permittivity $\varepsilon_{r1}=-\varepsilon_{r1p}<0$ and permeability $\mu_{r1}=-\mu_{r1p}<0$, whereas in medium 2 we assume $\varepsilon_{r2}>0$ and $\mu_{r2}>0$. The coordinate axes are chosen so that the z axis is directed along the SP propagation and the x axis is perpendicular to the media interface.

In what follows, we will examine p-polarized (TM) SP waves that exist due to the change in the sign of the permit-
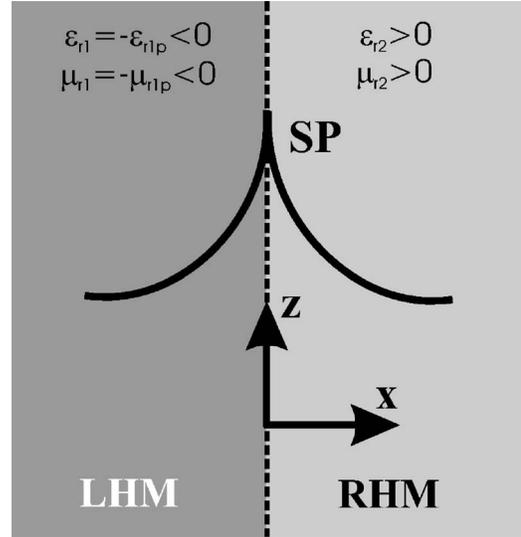

FIG. 1. Isolated interface between a left-handed material (LHM) and a right-handed material (RHM). The change in sign of the permittivity allows a p-polarized surface polariton (SP) to exist at this interface.

tivities. Analogous results can be obtained for s-polarized (TE) waves, following a dual analysis. The following relations describe the field components tangential to the interface of the media (in SI units):

$$\frac{d^2H_y}{dx^2} + (\varepsilon_r\mu_r k_0^2 - \beta^2)H_y = 0, \tag{1a}$$

$$E_z = -\frac{j}{\omega\varepsilon}\frac{\partial H_y}{\partial x}. \tag{1b}$$

Inside the LH medium, Eq. (1a) becomes

$$\frac{d^2H_y}{dx^2} - (\beta^2 - \varepsilon_{r1p}\mu_{r1p}k_0^2)H_y = 0 \tag{2}$$

where β is the longitudinal propagation constant of the SP wave. Assuming $\beta^2 > \max\{\varepsilon_{r1p}\mu_{r1p}k_0^2, \varepsilon_{r2}\mu_{r2}k_0^2\}$, the H_y-field component in medium 1 will be of the form $H_y=Ae^{\kappa x}$, where $\kappa=\sqrt{\beta^2-\varepsilon_{r1p}\mu_{r1p}k_0^2}$ and A is an arbitrary constant. For a bound wave to be supported by the interface, we seek H_y solutions that decay exponentially as $x\rightarrow\pm\infty$. Therefore, we seek a solution for medium 2 of the form $H_y=Ce^{-\gamma x}$. By direct substitution of this expression into the scalar wave equation for H_y in Eq. (1a) we obtain $\gamma=\sqrt{\beta^2-\varepsilon_{r2}\mu_{r2}k_0^2}$.

Applying the boundary conditions associated with the tangential H_y and E_z fields at $x=0$, yields a characteristic or eigenvalue equation for the formed SP at the plane interface that allows us to determine the conditions for its existence. In terms of the eigenmode's effective index $n_{\text{eff}}=\beta/k_0$, the aforementioned equation takes the form

$$n_{\text{eff}} = \left[\frac{\varepsilon_{r1p}\varepsilon_{r2}(\mu_{r1p}\varepsilon_{r2} - \mu_{r2}\varepsilon_{r1p})}{\varepsilon_{r2}^2 - \varepsilon_{r1p}^2}\right]^{1/2}. \tag{3}$$
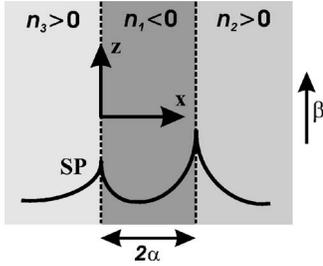
FIG. 2. Schematic representation of the asymmetric left-handed slab heterostructure. The core is a medium with negative refractive index n_1 and thickness 2α. Also shown is a possible field pattern of a supported SP and the direction of the longitudinal propagation constant β.

It is convenient for the subsequent discussions to rewrite Eq. (3) using the ratios of the permittivities, $\rho_\varepsilon = \varepsilon_{r2}/\varepsilon_{r1p}$, and permeabilities, $\rho_\mu = \mu_{r2}/\mu_{r1p}$, of the two media[17]

$$n_{\mathrm{eff}} = |n_1| \left[\frac{\rho_\varepsilon(\rho_\varepsilon - \rho_\mu)}{\rho_\varepsilon^2 - 1} \right]^{1/2}. \qquad (4)$$

Since ρ_ε is a positive quantity, we conclude from Eq. (4) that an SP at a LH/RH interface can only exist if

$$\{\rho_\varepsilon > 1 \quad \text{and} \quad \rho_\varepsilon > \rho_\mu\} \qquad (5a)$$

or

$$\{\rho_\varepsilon < 1 \quad \text{and} \quad \rho_\varepsilon < \rho_\mu\}. \qquad (5b)$$

Before closing this section, we wish to emphasize that these restrictions concern uncoupled ("unretarded") SPs existing at isolated LH/RH interfaces. We demonstrate in Sec. III that an SP eigenmode violating these constraints may exist if the interface that supports it, is brought sufficiently close to another LH/RH interface creating a "supermode," which is not obliged to obey the two different cases in Eq. (5).

III. SURFACE PLASMON POLARITONS IN ASYMMETRIC LH SLAB WAVEGUIDES

In the following we study surface plasmon polaritons propagating along a homogeneous isotropic slab of negative permittivity and permeability bounded by two different media with positive refractive indices, as illustrated in Fig. 2. The SPP eigenmodes in the slab waveguide will be travelling along the z direction. There is no variation in the guide geometry in the z direction and by symmetry no variation in the field distributions in the y direction. The thickness of the slab is 2α and in all the subsequent discussions we assume, without loss of generality, that $n_2 > n_3$.

In the analysis of planar dielectric waveguides,[19] the solution ansatz to the master equation is a monochromatic plane wave of frequency ω with a functional expression that can be symbolically written as

$$\Psi(x,z,t) = \Phi(x)e^{-j\beta z}e^{j\omega t}, \qquad (6)$$

where Ψ represents an electric or magnetic field component, Φ describes its amplitude in the x axis, and β is the longitu-

dinal component of the wave vector $\mathbf{k}$ in the slab. For TM SPPs, where the three existing field components are given by Eq. (1), we are seeking H_y-solutions in the three media, of the form

$$H_y(x) = \begin{cases} Ae^{\gamma_3 x}, & x \leq 0 \\ B\cosh(\kappa x) + C\sinh(\kappa x), & 0 \leq x \leq 2\alpha \\ De^{-(x-2\alpha)\gamma_2}, & x \geq 2\alpha, \end{cases} \qquad (7)$$

with $\kappa = \sqrt{\beta^2 - \varepsilon_{r1p}\mu_{r1p}k_0^2}$, $\gamma_2 = \sqrt{\beta^2 - \varepsilon_{r2}\mu_{r2}k_0^2}$, and $\gamma_3 = \sqrt{\beta^2 - \varepsilon_{r3}\mu_{r3}k_0^2}$, as in Sec. II. Similarly to the single interface case we require $n_{\mathrm{eff}} > \max\{|n_1|, n_2, n_3\}$, from which we make the ansatz to Eq. (7). By matching the tangential components at $x=0$ and $x=2\alpha$, we find

$$B = A, \qquad (8a)$$

$$C = -\frac{\varepsilon_{r1p}}{\varepsilon_{r3}}\frac{\gamma_3}{\kappa}A, \qquad (8b)$$

$$D = \left[\cosh(2\alpha\kappa) - \frac{\varepsilon_{r1p}}{\varepsilon_{r3}}\frac{\gamma_3}{\kappa}\sinh(2\alpha\kappa)\right]A, \qquad (8c)$$

and the following SPP characteristic equation is obtained:

$$\tanh(2\alpha\kappa) = \frac{\varepsilon_{r1p}\kappa(\varepsilon_{r3}\gamma_2 + \varepsilon_{r2}\gamma_3)}{\varepsilon_{r2}\varepsilon_{r3}\kappa^2 + \varepsilon_{r1p}^2\gamma_2\gamma_3}. \qquad (9)$$

As in classical fiber theory,[19] it is advantageous to introduce the following reduced, dimensionless, modal parameters:

$$U = \alpha\kappa = \alpha k_0\sqrt{n_{\mathrm{eff}}^2 - \varepsilon_{r1p}\mu_{r1p}}, \qquad (10a)$$

$$W_2 = \alpha\gamma_2 = \alpha k_0\sqrt{n_{\mathrm{eff}}^2 - \varepsilon_{r2}\mu_{r2}}, \qquad (10b)$$

$$W_3 = \alpha\gamma_3 = \alpha k_0\sqrt{n_{\mathrm{eff}}^2 - \varepsilon_{r3}\mu_{r3}}. \qquad (10c)$$

With these definitions, Eq. (9) takes the form

$$\tanh(2U) = \frac{\varepsilon_{r1p}U(\varepsilon_{r3}W_2 + \varepsilon_{r2}W_3)}{\varepsilon_{r2}\varepsilon_{r3}U^2 + \varepsilon_{r1p}^2W_2W_3}. \qquad (11)$$

In order to determine the power propagation direction, we calculate the time-averaged power flow in the slab heterostructure, obtained by the integral over the guide's cross section of the z component of the complex Poynting vector (S_z)

$$P = \int_{-\infty}^{\infty} S_z\,dx = \frac{1}{2}\int_{-\infty}^{\infty} \mathrm{Re}(\mathbf{E} \times \mathbf{H}^*)_z\,dx. \qquad (12)$$

For p-polarized SPP eigenmodes, S_z is given by

$$S_z = \frac{1}{2}H_y^*E_x = \frac{\beta}{2\omega\varepsilon_0\varepsilon_i}|H_y|^2 \quad (i = 1,2,3). \qquad (13)$$

From Eqs. (7)–(9), we find the power P_i confined in each region to be

$$P_3 = \left(\frac{A^2}{4\omega\varepsilon_0}\right)\frac{1}{\varepsilon_{r1p}}\frac{\beta}{\sigma_\varepsilon\gamma_3}, \qquad (14a)$$

TABLE I. Summary of the discussion for the case $|n_1| > n_2 > n_3$.

$\sigma_\varepsilon > 1$, $\rho_\varepsilon > 1$		$\sigma_\varepsilon > 1$, $\rho_\varepsilon \leqslant 1$	$\sigma_\varepsilon \leqslant 1$, $\rho_\varepsilon > 1$	$\sigma_\varepsilon \leqslant 1$, $\rho_\varepsilon \leqslant 1$
$\rho_\varepsilon > \sigma_\varepsilon$	$\rho_\varepsilon \in \Delta$			
First: forward, 2 cutoffs	First: backward, low cutoff	First: forward, 2 cutoffs	First: forward, 2 cutoffs	First: forward, upper cutoff
Second: backward, low cutoff	Second: backward, no cutoff	Second: backward, low cutoff	Second: backward, low cutoff	
Third: backward, no cutoff				

$$P_1 = -\left(\frac{A^2}{4\omega\varepsilon_0}\right)\frac{\beta}{\varepsilon_{r1p}}\frac{\sigma_\varepsilon^2\kappa^2 - \gamma_3^2}{\sigma_\varepsilon^2\kappa^2}\left[2\alpha + \frac{\rho_\varepsilon\gamma_2}{\rho_\varepsilon^2\kappa^2 - \gamma_2^2} + \frac{\sigma_\varepsilon\gamma_3}{\sigma_\varepsilon^2\kappa^2 - \gamma_3^2}\right],$$
(14b)

$$P_2 = \left(\frac{A^2}{4\omega\varepsilon_0}\right)\frac{\beta}{\varepsilon_{r1p}\rho_\varepsilon\gamma_2}\frac{\rho_\varepsilon^2}{\sigma_\varepsilon^2}\frac{\sigma_\varepsilon^2\kappa^2 - \gamma_3^2}{\rho_\varepsilon^2\kappa^2 - \gamma_2^2},$$
(14c)

where $\sigma_\varepsilon = \varepsilon_{r3}/\varepsilon_{r1p}$ and $\rho_\varepsilon = \varepsilon_{r2}/\varepsilon_{r1p}$. From Eq. (14) we can derive a closed-form expression for the total power $P_{\text{tot}} = \Sigma_{i=1}^3 P_i$ in terms of the dimensionless parameters defined in Eq. (10) and the reduced slab thickness αk_0

$$P_{\text{tot}} = \left(\frac{A^2}{4\omega\varepsilon_0}\right)\frac{W_3^2 - \sigma_\varepsilon^2 U^2}{\sigma_\varepsilon^2 U^2}\frac{(U^2 + \varepsilon_{r1p}\mu_{r1p}(\alpha k_0)^2)^{1/2}}{\varepsilon_{r1p}}$$
$$\times\left[2 + \frac{\rho_\varepsilon}{W_2}\frac{U^2 - W_2^2}{W_2^2 - \rho_\varepsilon^2 U^2} + \frac{\sigma_\varepsilon}{W_3}\frac{U^2 - W_3^2}{W_3^2 - \sigma_\varepsilon^2 U^2}\right].$$
(15)

The central task at this point is the determination of the solutions to Eq. (11). Their existence is identified following an analytical methodology. In what follows, we discuss the features and dependence of these solutions on the thickness of the inner layer, for the various cases of the refractive index distribution. A brief summary of the results for each case is found in Tables I–III.

A. Case I: $|n_1| > n_2 > n_3$

For this case, we start by defining the following two V-parameters:

$$V_2(\alpha k_0) = (W_2^2 - U^2)^{1/2} = \alpha k_0(\varepsilon_{r1p}\mu_{r1p} - \varepsilon_{r2}\mu_{r2})^{1/2},$$
(16a)

$$V_3(\alpha k_0) = (W_3^2 - U^2)^{1/2} = \alpha k_0(\varepsilon_{r1p}\mu_{r1p} - \varepsilon_{r3}\mu_{r3})^{1/2},$$
(16b)

where it is seen that the usual notation of the V number found in fiber theory[19] has been properly modified to accommodate the changes in the refractive index distribution and that both parameters are functions of αk_0. We also introduce the following ratios:

$$b(n_{\text{eff}}) = \frac{U}{V_2} = \left[\frac{(n_{\text{eff}}/n_1)^2 - 1}{1 - \rho_\varepsilon\rho_\mu}\right]^{1/2},$$
(17)

$$t = \frac{V_3}{V_2} = \left(\frac{1 - \sigma_\varepsilon\sigma_\mu}{1 - \rho_\varepsilon\rho_\mu}\right)^{1/2},$$
(18)

obeying the restrictions $b > 0$ and $t > 1$, where $\rho_\mu = \mu_{r2}/\mu_{r1p}$ and $\sigma_\mu = \mu_{r3}/\mu_{r1p}$. Note that similar ratios to b and t are utilized in the analysis of conventional slab waveguides to denote the "normalized guide index" and the "asymmetry measure," respectively,[20] and that b is a function of the SPP eigenmode's effective index.

For the explicit acquisition of the dispersion diagrams and the derivation of the analytical restrictions inherent in Eq. (11), a common strategy is to produce an inverted version of the associated characteristic equation.[15,20] First, we note from Eqs. (16) and (17) that $U = bV_2$, $W_2 = V_2(b^2+1)^{1/2}$ and $W_3 = V_2(b^2+t^2)^{1/2}$. With these observations, Eq. (11) can be rewritten in the form

$$V_2 = \frac{1}{4b}\ln\left[\frac{(X+1)(Y+1)}{(X-1)(Y-1)}\right],$$
(19)

where $X(b) = \sigma_\varepsilon b/(b^2+t^2)^{1/2}$ and $Y(b) = \rho_\varepsilon b/(b^2+1)^{1/2}$. Since V_2, given in Eq. (16a), is a real number, we immediately see that Eq. (19) only has solutions, when the argument of the logarithm is positive, i.e., for

TABLE II. Summary of the discussion for the case $n_2 > n_3 > |n_1|$.

$\sigma_\varepsilon \geqslant 1$, $\rho_\varepsilon \geqslant 1$	$\sigma_\varepsilon \geqslant 1$, $\rho_\varepsilon < 1$	$\sigma_\varepsilon < 1$, $\rho_\varepsilon \geqslant 1$	$\sigma_\varepsilon < 1$, $\rho_\varepsilon < 1$		
			$\rho_\varepsilon \in \Delta$	$\rho_\varepsilon \in \Delta'$	$\rho_\varepsilon\rho_\mu > (\sigma_\varepsilon\sigma_\mu - \sigma_\varepsilon^2)/(1-\sigma_\varepsilon^2)$
First: forward, 2 cutoffs	First: forward, low cutoff	First: forward, low cutoff	First: forward, low cutoff	First: forward, low cutoff	First: forward, no cutoff
Second: backward, upper cutoff			Second: forward, no cutoff	Second: forward, no cutoff	

$$\{X > 1 \quad \text{and} \quad Y > 1\}, \tag{20a}$$

or:

$$\{0 < X < 1 \quad \text{and} \quad 0 < Y < 1\}. \tag{20b}$$

We now examine, in detail, the consequences of these restrictions on $X(b)$ and $Y(b)$, based on which the existing SPP eigenmodes are rigorously identified. In particular, we derive analytically the allowable range of values that b, hence the eigenmodes' effective index, can take. In pursuing this analysis, we find that it is necessary to distinguish between the following four situations that describe the possible variations in the permittivity distribution. In all four of them, it is implied that $\sigma_\varepsilon \sigma_\mu < \rho_\varepsilon \rho_\mu < 1$ from the initial assumption $|n_1| > n_2 > n_3$.

The first situation occurs for $\{\sigma_\varepsilon > 1 \text{ and } \rho_\varepsilon > 1\}$. When $\rho_\varepsilon > \sigma_\varepsilon$, inspection of Eq. (20) results in the allowable values for b; that is $0 < b < b_1$ or $b > b_2$, where

$$b_1 = \left(\frac{1}{\rho_\varepsilon^2 - 1}\right)^{1/2}, \tag{21}$$

and

$$b_2 = \left[\frac{1 - \sigma_\varepsilon \sigma_\mu}{(\sigma_\varepsilon^2 - 1)(1 - \rho_\varepsilon \rho_\mu)}\right]^{1/2}. \tag{22}$$

The corresponding geometric dispersion diagram is shown in Fig. 3(a), and the variation of the normalized power $P = P_{tot}/(|P_1| + |P_2| + |P_3|)$ (Ref. 11) with the reduced slab thickness for each solution is given in Fig. 3(b). Three SPP eigenmodes exist in this case. The first has a lower cutoff and an upper one at $b = 0$, is forward propagating, having positive total power P, and the field intensity has a node in the core region. It should be noted that modes with oscillating field inside the core can also exist in high-index guiding LH structures.[11] Therefore, all SPP cutoff points corresponding to $b = 0$ are not necessarily "real" cutoffs where no electromagnetic mode (SPP or oscillatory) can exist any more, but a transition point from SPP mode to oscillatory mode. It is worth pointing out that for all SPPs considered in case I this continuous transformation is into the first oscillating mode.

At the lower cutoff point, the previous SPP solution degenerates into the second eigenmode. This SPP has a low cutoff and no upper cutoff and is backward propagating, having negative energy velocity and, since the dielectric media are nonabsorbing, negative group velocity, as well.[21] After a finite gap, a third eigenmode appears, which has no cutoff and is also backward propagating having negative P for every core thickness. The corresponding fields have no node in the core region.

It is interesting to discuss the behavior of these solutions in the extreme cases of $b \to b_1$ and $b \to b_2$. First, by letting b become equal to b_1, we recover asymptotically Eq. (4), which is the SPP characteristic equation at the 1-2 media interface. Such result is expected, since from Eqs. (16a) and (19) and from Fig. 3(a) we note that for $b \to b_1, \alpha k_0 \to \infty$, hence the two slab interfaces decouple and the SPP at an isolated interface should be recovered. For a relatively large value of αk_0, the result of plotting this SPP eigenmode is shown in the middle left inset of Fig. 3(a), reflecting the previous conclusions. Then, assuming that $b = b_2$, we obtain

$$n_{\mathrm{eff},3} = |n_1| \left[\frac{\sigma_\varepsilon(\sigma_\varepsilon - \sigma_\mu)}{\sigma_\varepsilon^2 - 1}\right]^{1/2}, \tag{23}$$

and the SPP eigenmode at the 1-3 interface is recovered asymptotically, shown in the top inset.

When $\rho_\varepsilon < \sigma_\varepsilon$, it proves necessary to examine the intervals that to which the ratio ρ_ε belongs. If $\rho_\varepsilon \in \Delta$, where $\Delta = \{(\rho_{\varepsilon,1} < \rho_\varepsilon < \rho_{\varepsilon,2}) \cap (\rho_\varepsilon > 1)\}$ and $\rho_{\varepsilon,1}, \rho_{\varepsilon,2}$ are the two roots of the polynomial

$$\Pi(\rho_\varepsilon) = (1 - \sigma_\varepsilon \sigma_\mu)\rho_\varepsilon^2 + \rho_\mu(\sigma_\varepsilon^2 - 1)\rho_\varepsilon - [(1 - \sigma_\varepsilon \sigma_\mu) + (\sigma_\varepsilon^2 - 1)], \tag{24}$$

it is $b_1 > b_2$, and we see from Fig. 3(c) that two eigenmodes exist, both of which are backward propagating. The first SPP has only a lower cutoff at $b = 0$ and, contrary to the previous case, it concentrates asymptotically at the 1-3 interface while exhibiting a phase reversal. The second (upper) SPP shows no cutoff, has positive H_y-field component throughout the slab and concentrates at the 1-2 media interface for large core thickness. For $\rho_\varepsilon \in \Delta'$, where $\Delta' = \{[(\rho_\varepsilon < \rho_{\varepsilon,1}) \cup (\rho_\varepsilon > \rho_{\varepsilon,2})] \cap (\rho_\varepsilon > 1)\}$, we have $b_1 < b_2$ and the results of the analysis hold the same as in the case $\rho_\varepsilon > \sigma_\varepsilon$, apart from the disappearance of the first SPP eigenmode that was forward propagating.

The second situation occurs for $\{\sigma_\varepsilon > 1 \text{ and } \rho_\varepsilon \leq 1\}$. From the conditions in Eq. (20), we find that b ranges from 0 to b_2 and the corresponding dispersion diagram is illustrated in Fig. 3(e). In this case two eigenmodes are shown to exist; for both, the H_y component has a node in the core region. The first has a low cutoff and an upper one occurring at $b = 0$, and

TABLE III. Summary of the discussion for the case $n_2 > |n_1| > n_3$.

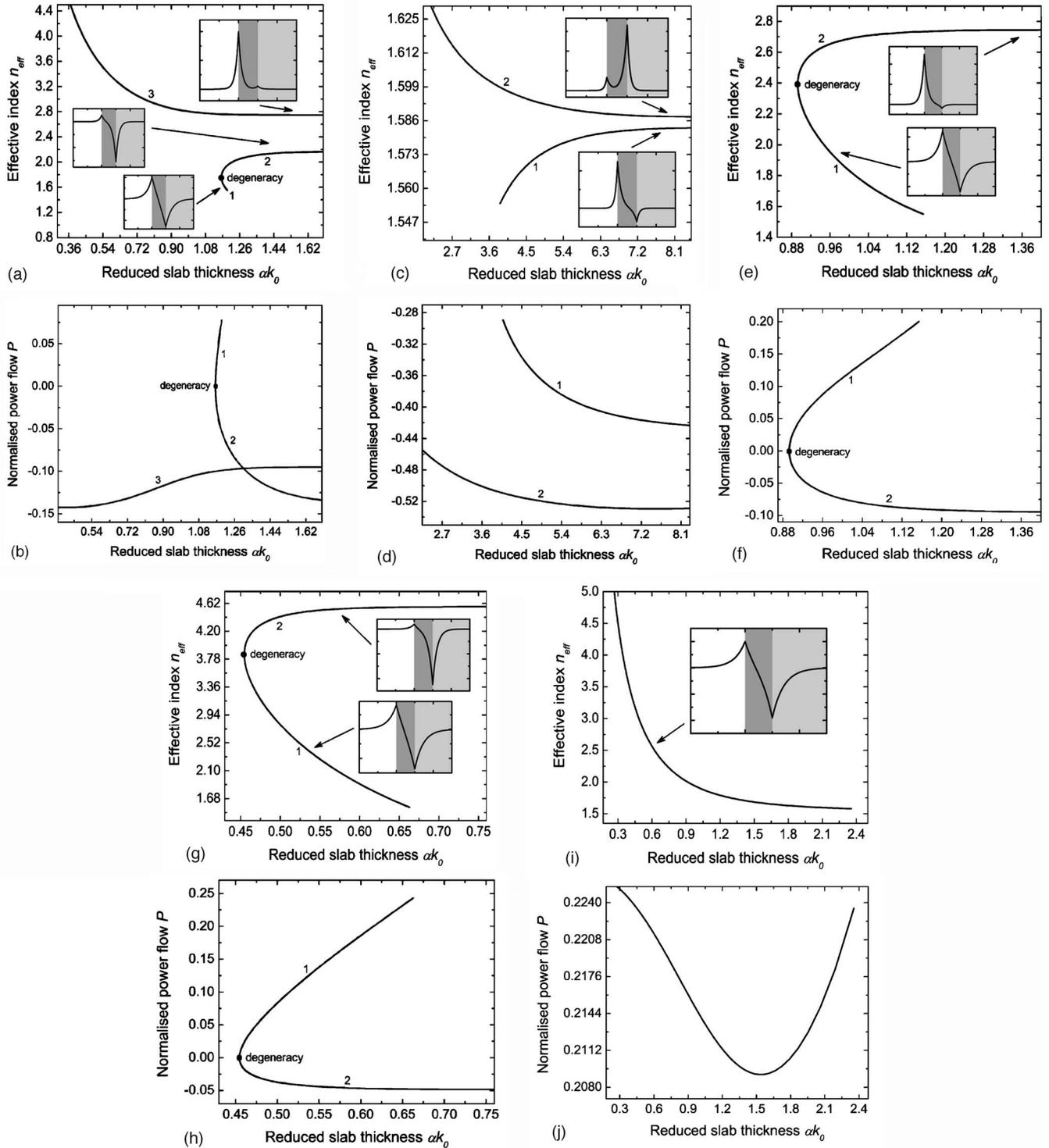| $\sigma_\varepsilon > 1$, $\rho_\varepsilon \geq 1$			$\sigma_\varepsilon > 1$, $\rho_\varepsilon < 1$			$\sigma_\varepsilon \leq 1$, $\rho_\varepsilon < 1$
$\rho_\varepsilon\rho_\mu < (\sigma_\varepsilon^2 - \sigma_\varepsilon\sigma_\mu)/(\sigma_\varepsilon^2 - 1)$	$\rho_\varepsilon\rho_\mu > (\sigma_\varepsilon^2 - \sigma_\varepsilon\sigma_\mu)/(\sigma_\varepsilon^2 - 1)$	$\rho_\varepsilon \in \Delta$	$\rho_\varepsilon \in \Delta'$	$\rho_\varepsilon\rho_\mu > (\sigma_\varepsilon^2 - \sigma_\varepsilon\sigma_\mu)/(\sigma_\varepsilon^2 - 1)$		
First: backward, no cutoff	First: forward, 2 cutoffs	First: backward, low cutoff	First: forward, low cutoff	First: forward, 2 cutoffs		First: forward, no cutoff
	Second: backward, upper cutoff	Second: forward, low cutoff	Second: backward, low cutoff	Second: backward, 2 cutoffs		
				Third: forward, low cutoff		

FIG. 3. Variation of an SP eigenmode's effective index n_{eff} and normalized power P with the reduced slab thickness αk_0 in a generalized LH slab waveguide (case I: $|n_1| > n_2 > n_3$, as indicated by the shaded background). In all cases it is assumed that $\varepsilon_r = 2$, $\mu_r = 1.2$. (a), (b) n_{eff} and P variation for $\sigma_\varepsilon = 1.1$, $\sigma_\mu = 0.5$, $\rho_\varepsilon = 1.15$, $\rho_\mu = 0.6$. (c), (d) Variations for $\sigma_\varepsilon = 1.8$, $\sigma_\mu = 0.5$, $\rho_\varepsilon = 1.55$, $\rho_\mu = 0.6$. (e), (f) Variations for $\sigma_\varepsilon = 1.1$, $\sigma_\mu = 0.5$, $\rho_\varepsilon = 0.95$, $\rho_\mu = 0.8$. (g), (h) Variations for $\sigma_\varepsilon = 0.8$, $\sigma_\mu = 0.2$, $\rho_\varepsilon = 1.05$, $\rho_\mu = 0.2$. (i), (j) Variations for $\sigma_\varepsilon = 0.8$, $\sigma_\mu = 1$, $\rho_\varepsilon = 0.9$, $\rho_\mu = 1.1$.

is forward propagating. The second SPP has only a low cut-off and it concentrates asymptotically at the 1-3 interface. As in all the encountered cases that contain degeneracy, the total power P at this point equals zero, corresponding to zero

group velocity. Waves with this feature are of great practical interest for optical communication and data storage applications.[22] It should be noted that, for the particular values of the permittivity and permeability ratios shown in

Fig. 3(e), the 1-2 single interface does not support an SPP because the constraints in Eq. (5) are violated. However, the coupled SPPs at the interfaces of the slab overcome this limitation, creating the two new SPP "supermodes" for relatively large slab thickness.

In the third case, which exists for $\{\sigma_\varepsilon \leqslant 1$ and $\rho_\varepsilon > 1\}$, it is found that the range of values for b is between 0 and b_1. The variation of the eigenmodes' effective index and power with the reduced guide thickness is shown in Figs. 3(g) and 3(h). The conclusions for the supported SPPs are similar with those in the previous case, with the difference that the second (upper) eigenmode concentrates asymptotically at the 1-2 interface while taking negative values. In this case also, it is the 1-3 interface that violates the SPP existence conditions and, if isolated, would not support a bound wave.

The final situation occurs for $\{\sigma_\varepsilon \leqslant 1$ and $\rho_\varepsilon \leqslant 1\}$. In this case there are no additional restrictions on b other than $b > 0$. From Figs. 3(i) and 3(j) we see that only one SPP eigenmode exists, which is forward propagating with only a higher cutoff at $b=0$ and has opposite sign at the two interfaces of the slab.

B. Case II: $n_2 > n_3 > |n_1|$

For the refractive index distribution considered here, we use the following definitions for the V numbers:

$$V_2(\alpha k_0) = (U^2 - W_2^2)^{1/2} = \alpha k_0 (\varepsilon_{r2}\mu_{r2} - \varepsilon_{r1p}\mu_{r1p})^{1/2},$$
(25a)

$$V_3(\alpha k_0) = (U^2 - W_3^2)^{1/2} = \alpha k_0 (\varepsilon_{r3}\mu_{r3} - \varepsilon_{r1p}\mu_{r1p})^{1/2},$$
(25b)

with $\rho_\varepsilon \rho_\mu > \sigma_\varepsilon \sigma_\mu > 1$ used throughout the following analysis. Then, the previously introduced b and t parameters take the form

$$b(n_{\text{eff}}) = \frac{U}{V_2} = \left[\frac{(n_{\text{eff}}/n_1)^2 - 1}{\rho_\varepsilon \rho_\mu - 1} \right]^{1/2},$$
(26)

$$t = \frac{V_3}{V_2} = \left(\frac{\sigma_\varepsilon \sigma_\mu - 1}{\rho_\varepsilon \rho_\mu - 1} \right)^{1/2},$$
(27)

obeying the restrictions $b > 1$ and $t < 1$. The general form of Eq. (19) and the solution conditions of Eq. (20) remain the same, but now we have $W_2 = V_2(b^2 - 1)^{1/2}$, $W_3 = V_2(b^2 - t^2)^{1/2}$, $X(b) = \sigma_\varepsilon b/(b^2 - t^2)^{1/2}$ and $Y(b) = \rho_\varepsilon b/(b^2 - 1)^{1/2}$. By letting $X(b)$ and $Y(b)$ fulfill these conditions, we again find that four distinct situations arise depending on the permittivity profile.

The first situation occurs for $\{\sigma_\varepsilon \geqslant 1$ and $\rho_\varepsilon \geqslant 1\}$, and does not contain further restrictions on b. The eigenmodes' effective index and P dispersion diagrams are shown in Figs. 4(a) and 4(b). We see that two SPPs exist; both have no node in the middle layer. The first, which is forward propagating, has a lower cutoff at $b=1$ and also an upper cutoff point, where it degenerates into the second eigenmode. The second SPP has only a high cutoff and is backward propagating having negative total power P.

The second situation occurs for $\{\sigma_\varepsilon \geqslant 1$ and $\rho_\varepsilon < 1\}$, and it can be shown that b is in the range $1 < b < b_1$, where now

$$b_1 = \left(\frac{1}{1 - \rho_\varepsilon^2} \right)^{1/2}.$$
(28)

In this case, a single SPP eigenmode is shown to exist, having only a low cutoff at $b=1$. This SPP is forward propagating and concentrates at the 1-2 media interface for large core thickness, as illustrated in the inset of Fig. 4(c). This result is also verified by letting $b=b_1$, where we obtain the SPP characteristic Eq. (4).

The third case exists for $\{\sigma_\varepsilon < 1$ and $\rho_\varepsilon \geqslant 1\}$, and it is found that b ranges from 1 to b_2, where now

$$b_2 = \left[\frac{\sigma_\varepsilon \sigma_\mu - 1}{(1 - \sigma_\varepsilon^2)(\rho_\varepsilon \rho_\mu - 1)} \right]^{1/2},$$
(29)

with the constraint $\rho_\varepsilon \rho_\mu < (\sigma_\varepsilon \sigma_\mu - \sigma_\varepsilon^2)/(1 - \sigma_\varepsilon^2)$. The variation of the effective index and total power with the reduced guide thickness are shown in Figs. 4(e) and 4(f). The conclusions are similar with the previous case, with the difference that the supported SPP concentrates asymptotically at the 1-3 interface. For the values of ρ_ε and ρ_μ shown in Fig. 4(e), the isolated 1-2 interface would not support an SPP.

The final situation occurs for $\{\sigma_\varepsilon < 1$ and $\rho_\varepsilon < 1\}$. If $\rho_\varepsilon \rho_\mu < (\sigma_\varepsilon \sigma_\mu - \sigma_\varepsilon^2)/(1 - \sigma_\varepsilon^2)$, it proves necessary to examine the intervals that the ratio ρ_ε belongs to. When $\rho_\varepsilon \in \Delta$, with $\Delta = \{[(\rho_\varepsilon < \rho_{\varepsilon,1}) \cup (\rho_\varepsilon > \rho_{\varepsilon,2})] \cap (0 < \rho_\varepsilon < 1)\}$ and $\rho_{\varepsilon,1}, \rho_{\varepsilon,2}$ being the two roots of the polynomial

$$\Pi(\rho_\varepsilon) = (\sigma_\varepsilon \sigma_\mu - 1)\rho_\varepsilon^2 + \rho_\mu(1 - \sigma_\varepsilon^2)\rho_\varepsilon - [(1 - \sigma_\varepsilon^2)$$
$$+ (\sigma_\varepsilon \sigma_\mu - 1)],$$
(30)

it is $b_1 > b_2$, and we see from Fig. 4(g) that two eigenmodes exist, both of which are forward propagating. The first SPP has only a low cutoff at $b=1$ and concentrates asymptotically at the 1-3 interface; the corresponding field intensity has no node in the core region. The second SPP has no cutoff, exhibits phase reversal and concentrates at the 1-2 media interface for large core thickness. For $\rho_\varepsilon \in \Delta'$, where $\Delta' = \{(\rho_{\varepsilon,1} < \rho_\varepsilon < \rho_{\varepsilon,2}) \cap (0 < \rho_\varepsilon < 1)\}$, we have $b_1 < b_2$ and again two SPP eigenmodes are shown to exist in Figs. 4(i) and 4(j). The first has positive H_y-field amplitude across the slab. Compared to the previous two eigenmodes, the cutoff characteristics remain the same, but the order of the interfaces to which these SPPs concentrate is reversed. Finally, if $\rho_\varepsilon \rho_\mu > (\sigma_\varepsilon \sigma_\mu - \sigma_\varepsilon^2)/(1 - \sigma_\varepsilon^2)$, the constraint $b > b_1$ becomes mandatory. The dispersion diagrams for this case are shown in Figs. 4(k) and 4(l). We see that a single SPP exists, which shows no cutoff, exhibits phase reversal, concentrates asymptotically at the 1-2 interface and has positive total power for all core thicknesses.

C. Case III: $n_2 > |n_1| > n_3$

To reflect the refractive index distribution considered here, the two V numbers are defined as

$$V_2(\alpha k_0) = (U^2 - W_2^2)^{1/2} = \alpha k_0 (\varepsilon_{r2}\mu_{r2} - \varepsilon_{r1p}\mu_{r1p})^{1/2},$$
(31a)

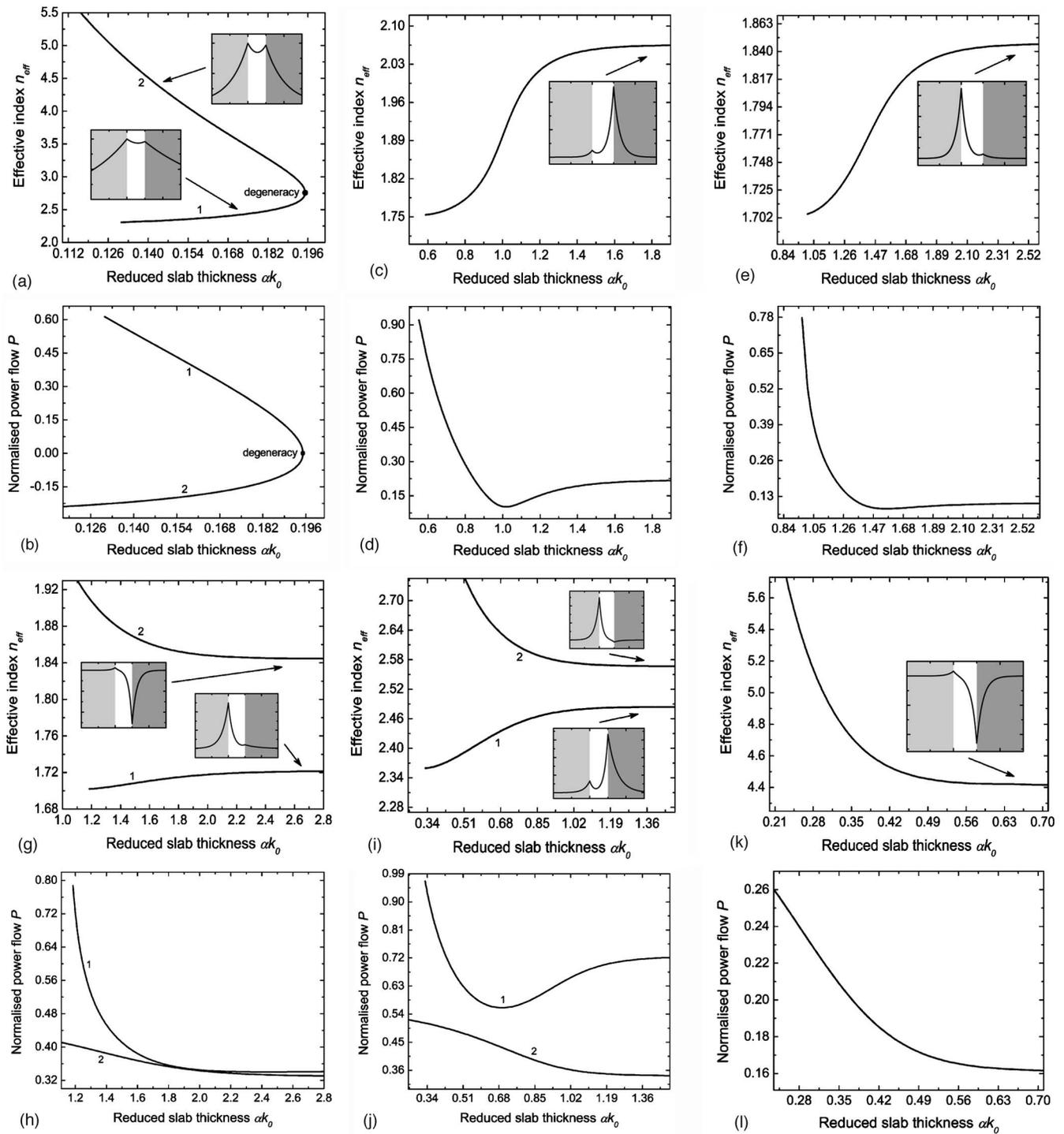FIG. 4. Variation of an SP eigenmode's effective index n_{eff} and normalized power P with the reduced slab thickness αk_0 in a generalized LH slab waveguide (case II: $n_2 > n_3 > |n_1|$, as indicated by the shaded background). In all cases, it is assumed that $\varepsilon_r = 2$, $\mu_r = 1.2$. (a), (b) n_{eff} and P variation for $\sigma_\varepsilon = 1.7$, $\sigma_\mu = 1.1$, $\rho_\varepsilon = 1.8$, $\rho_\mu = 1.2$. (c), (d) Variations for $\sigma_\varepsilon = 1.2$, $\sigma_\mu = 0.9$, $\rho_\varepsilon = 0.8$, $\rho_\mu = 1.6$. (e), (f) Variations for $\sigma_\varepsilon = 0.9$, $\sigma_\mu = 1.2$, $\rho_\varepsilon = 1.1$, $\rho_\mu = 1.1$. (g), (h) Variations for $\sigma_\varepsilon = 0.7$, $\sigma_\mu = 1.6$, $\rho_\varepsilon = 0.71$, $\rho_\mu = 1.7$. (i), (j) Variations for $\sigma_\varepsilon = 0.7$, $\sigma_\mu = 2.7$, $\rho_\varepsilon = 0.4$, $\rho_\mu = 5.8$. (k), (l) Variations for $\sigma_\varepsilon = 0.7$, $\sigma_\mu = 2.7$, $\rho_\varepsilon = 0.85$, $\rho_\mu = 3.5$.

$$V_3(\alpha k_0) = (W_3^2 - U^2)^{1/2} = \alpha k_0 (\varepsilon_{r1p}\mu_{r1p} - \varepsilon_{r3}\mu_{r3})^{1/2},$$
(31b)

with $\rho_\varepsilon\rho_\mu > 1 > \sigma_\varepsilon\sigma_\mu$ used in the remaining analysis. Accordingly, the b and t ratios take the form

$$b(n_{\text{eff}}) = \frac{U}{V_2} = \left[\frac{(n_{\text{eff}}/n_1)^2 - 1}{\rho_\varepsilon\rho_\mu - 1}\right]^{1/2},$$
(32)

$$t = \frac{V_3}{V_2} = \left(\frac{1 - \sigma_\varepsilon\sigma_\mu}{\rho_\varepsilon\rho_\mu - 1}\right)^{1/2},$$
(33)

obeying the restrictions $b > 1$ and $t > 0$. Once more, the general form of Eq. (19) and the solution conditions of Eq. (20) remain the same, but now $W_2 = V_2(b^2 - 1)^{1/2}$, $W_3 = V_2(b^2 + t^2)^{1/2}$, $X(b) = \sigma_\varepsilon b/(b^2 + t^2)^{1/2}$ and $Y(b) = \rho_\varepsilon b/(b^2 - 1)^{1/2}$. By letting $X(b)$ and $Y(b)$ fulfill the aforesaid conditions, the following four distinct situations arise depending on the permittivity profile.

The first situation occurs for $\{\sigma_\varepsilon > 1$ and $\rho_\varepsilon \geq 1\}$. If $\rho_\varepsilon\rho_\mu < (\sigma_\varepsilon^2 - \sigma_\varepsilon\sigma_\mu)/(\sigma_\varepsilon^2 - 1)$, the allowable range of values for b is $b > b_2$, where

$$b_2 = \left[\frac{1 - \sigma_\varepsilon\sigma_\mu}{(\rho_\varepsilon\rho_\mu - 1)(\sigma_\varepsilon^2 - 1)}\right]^{1/2}.$$
(34)

We see from Figs. 5(a) and 5(b) that a single eigenmode exists, which is backward propagating and has no cutoff. For large core thickness, the SPP characteristic equation at the 1-3 interface is recovered. The other interface would not support a SPP, if isolated. In the case $\rho_\varepsilon\rho_\mu > (\sigma_\varepsilon^2 - \sigma_\varepsilon\sigma_\mu)/(\sigma_\varepsilon^2 - 1)$, it is seen from Figs. 5(c) and 5(d) that two SPP eigenmodes can exist; both have no node in the inner layer. The first one, which is forward propagating, has a low cutoff point at $b = 1$ and a high cutoff, where it degenerates into the second SPP. This eigenmode is backward propagating having only an upper cutoff.

The second situation is described by $\{\sigma_\varepsilon > 1$ and $\rho_\varepsilon < 1\}$. For $\rho_\varepsilon\rho_\mu < (\sigma_\varepsilon^2 - \sigma_\varepsilon\sigma_\mu)/(\sigma_\varepsilon^2 - 1)$, it proves necessary to examine the intervals that the ratio ρ_ε belong to. When $\rho_\varepsilon \in \Delta$, with $\Delta = \{[(\rho_\varepsilon < \rho_{\varepsilon,1}) \cup (\rho_\varepsilon > \rho_{\varepsilon,2})] \cap (0 < \rho_\varepsilon < 1)\}$ and $\rho_{\varepsilon,1}$, $\rho_{\varepsilon,2}$ being the two roots of the polynomial

$$\Pi(\rho_\varepsilon) = (1 - \sigma_\varepsilon\sigma_\mu)\rho_\varepsilon^2 + \rho_\mu(\sigma_\varepsilon^2 - 1)\rho_\varepsilon - [(1 - \sigma_\varepsilon^2) + (1 - \sigma_\varepsilon\sigma_\mu)],$$
(35)

it is $b_1 > b_2$, where

$$b_1 = \left(\frac{1}{1 - \rho_\varepsilon^2}\right)^{1/2},$$
(36)

and it can be shown that b is in the range $b_2 < b < b_1$. The corresponding dispersion diagrams are illustrated in Figs. 5(e) and 5(f). We see that two nodeless eigenmodes exist. The first one has only a low cutoff, is backward propagating and concentrates asymptotically at the 1-3 interface. The second SPP has only a low cutoff, is forward propagating and concentrates at the 1-2 interface for relatively large core thicknesses. For $\rho_\varepsilon \in \Delta'$, where $\Delta' = \{(\rho_{\varepsilon,1} < \rho_\varepsilon < \rho_{\varepsilon,2}) \cap (0 < \rho_\varepsilon < 1)\}$, it is $b_1 < b_2$ and again two SPP eigen-

modes are shown to exist in Figs. 5(g) and 5(h). Compared to the previous two eigenmodes, the cutoff characteristics and the classification remain the same, but the order of the interfaces to which these SPPs concentrate is reversed. Also, both SPPs now exhibit phase reversal. For $\rho_\varepsilon\rho_\mu > (\sigma_\varepsilon^2 - \sigma_\varepsilon\sigma_\mu)/(\sigma_\varepsilon^2 - 1)$, we have $1 < b < b_1$ and the dispersion diagrams are shown in Figs. 5(i) and 5(j). In this case, three distinct solutions of Eq. (11) are found; the H_y-field intensity for all of them has no node in the core region. The first one, which corresponds to positive total power P, has a low cutoff point at $b = 1$ and an upper cutoff, where it degenerates into the second SPP. This eigenmode has also a lower and a higher cutoff, but is backward propagating. The third branch shows only a low cutoff, corresponds to positive P and, asymptotically, degenerates into the isolated 1-2 interface solution. This situation is the only one where two double mode-degeneracy points occur.

In the third situation, which occurs for $\{\sigma_\varepsilon < 1$ and $\rho_\varepsilon > 1\}$, there are no solutions to Eq. (19) for any $b > 1$; hence, the slab waveguide does not support SPPs.

The final situation occurs for $\{\sigma_\varepsilon \leq 1$ and $\rho_\varepsilon < 1\}$ and the corresponding dispersion diagrams are shown in Figs. 5(k) and 5(l). From the solution constraints of Eq. (20), we find that $b > b_1$. A single SPP exists, which does not have cutoff, is forward propagating, exhibits phase reversal and concentrates asymptotically at the 1-2 media interface. It should be noted that, for the chosen values of σ_ε and σ_μ, the isolated 1-3 interface does not support an SPP.

IV. CONCLUSIONS

We have presented a systematic investigation of all solutions of the involved characteristic equation giving the p-polarized surface plasmon polariton eigenmodes in generalized slab waveguides, comprised of a negative refractive index core that is bounded by two different positive-index media. Following an analytical methodology, all SPPs are classified as forward or backward propagating, depending on the sign of the associated power flow. Contrary to the case of thin metallic films surrounded by two different dielectrics, where the SPPs depend solely on the permittivity distribution, we have shown analytically that, for the corresponding left-handed structures considered here, the refractive index distribution must also be included in the analysis.

In particular, if the absolute value of the core refractive index is greater than those of the surrounding dielectrics, we identified ten TM SPP eigenmodes; six of these solutions are backward propagating. Nine solutions existed if the core index has the smallest absolute value; one of these SPPs has antiparallel phase and group velocities. In the final case, where the core index value is between those of the claddings, 11 SPP eigenmodes were identified; five of these solutions have backward power flow in relation to the direction of the phase velocity. The total number of 30 SPP eigenmodes, which is significantly higher than the six SPPs that were recognized in similar metallic film geometries,[15] is a direct result of the presence of negative magnetic permeability in the LH structures that provides additional degrees of freedom in the definition of the V numbers.
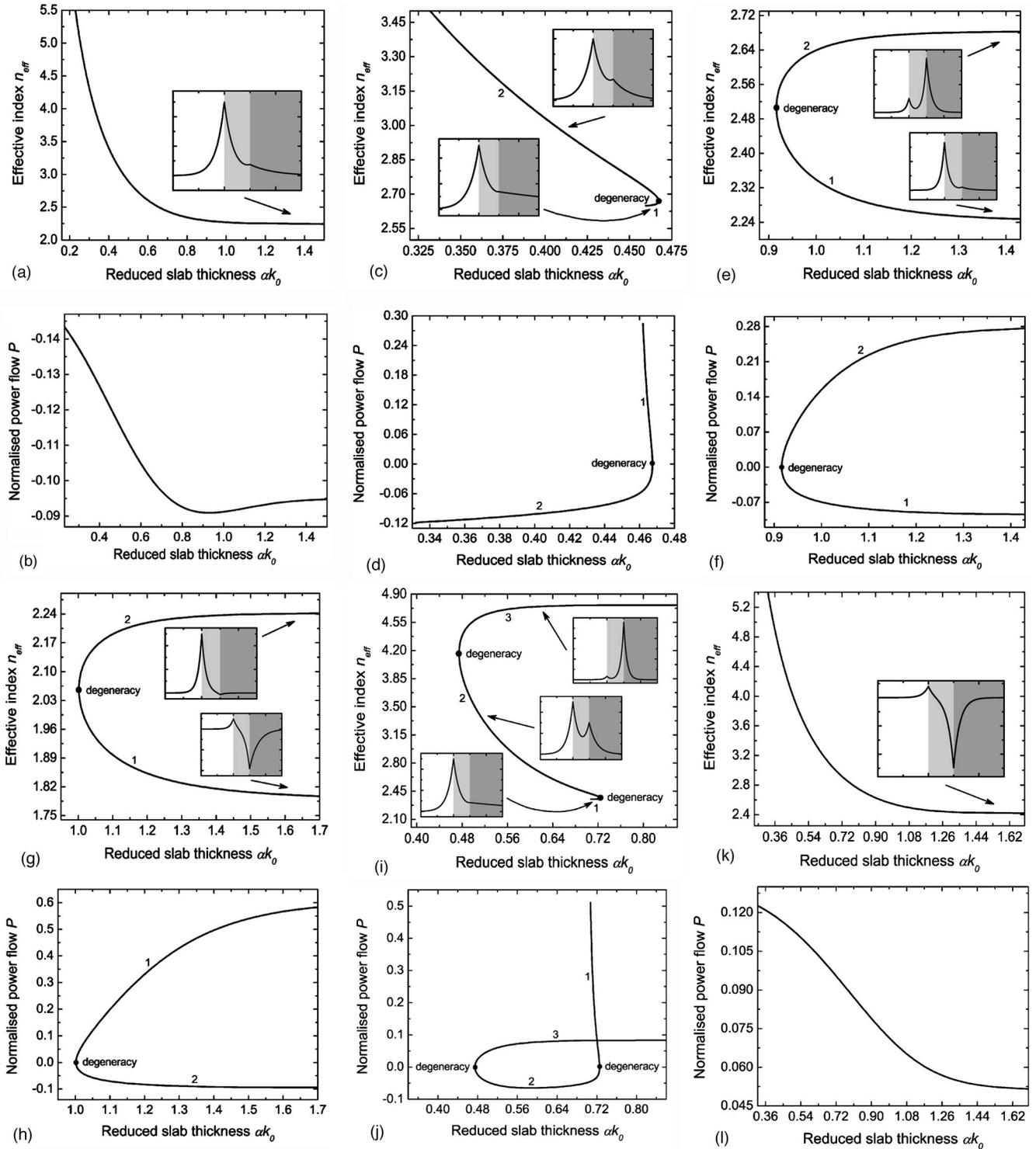
FIG. 5. Variation of an SP eigenmode's effective index n_{eff} and normalized power P with the reduced slab thickness αk_0 in a generalized LH slab waveguide (case III: $n_2 > |n_1| > n_3$, as indicated by the shaded background). In all cases it is assumed that $\varepsilon_r = 2$, $\mu_r = 1.2$. (a), (b) n_{eff} and P variation for $\sigma_\varepsilon = 1.1$, $\sigma_\mu = 0.7$, $\rho_\varepsilon = 1.38$, $\rho_\mu = 1.5$. (c), (d) Variations for $\sigma_\varepsilon = 1.1$, $\sigma_\mu = 0.7$, $\rho_\varepsilon = 1.95$, $\rho_\mu = 1.5$. (e), (f) Variations $\sigma_\varepsilon = 1.1$, $\sigma_\mu = 0.7$, $\rho_\varepsilon = 0.75$, $\rho_\mu = 2.5$. (g), (h) Variations for $\sigma_\varepsilon = 1.1$, $\sigma_\mu = 0.7$, $\rho_\varepsilon = 0.5$, $\rho_\mu = 2.5$. (i), (j) Variations for $\sigma_\varepsilon = 1.1$, $\sigma_\mu = 0.7$, $\rho_\varepsilon = 0.92$, $\rho_\mu = 2.5$. (k), (l) Variations for $\sigma_\varepsilon = 0.9$, $\sigma_\mu = 0.9$, $\rho_\varepsilon = 0.95$, $\rho_\mu = 1.2$.

The analytical treatment revealed features not observed before, such as the occurrence of "supermodes" in the case of a violation of the isolated interface condition, strong field enhancement and opening of gaps in the geometric dispersion diagrams owing to the asymmetry, and coexistence of three eigenmodes with double mode-degeneracy points occurring twice. We also demonstrated that the group velocity of the investigated slow waves could be decreased down to zero or become negative, by adjusting suitably the thickness of the core.

[1] V. G. Veselago, Sov. Phys. Usp. **10**, 509 (1968); V. G. Veselago, in *Proceedings of the First Taormina Research Conference on the Structure of Matter, Pergamon, 1972*, edited by E. Burstein and F. De Martini (Pergamon Press, New York, 1974), p. 5.

[2] P. M. Valanju, R. M. Walser, and A. P. Valanju, Phys. Rev. Lett. **88**, 187401 (2002).

[3] J. B. Pendry, Phys. Rev. Lett. **85**, 3966 (2000).

[4] N. Garcia and M. Nieto-Vesperinas, Phys. Rev. Lett. **88**, 207403 (2002).

[5] D. R. Smith, D. Schurig, and J. B. Pendry, Appl. Phys. Lett. **81**, 2713 (2002); D. R. Smith, D. Schurig, M. Rosenbluth, S. Schultz, S. A. Ramakrishna, and J. B. Pendry, *ibid.* **82**, 1506 (2003).

[6] S. A. Cummer, Appl. Phys. Lett. **82**, 2008 (2003); W. T. Lu, J. B. Sokoloff, and S. Sridhar, Phys. Rev. E **69**, 026604 (2004).

[7] C. G. Parazzoli, R. B. Greegor, K. Li, B. E. C. Koltenbah, and M. Tanielian, Phys. Rev. Lett. **90**, 107401 (2003); A. A. Houck, J. B. Brock, and I. L. Chuang, *ibid.* **90**, 137401 (2003).

[8] J. B. Pendry, A. J. Holden, W. J. Stewart, and I. Youngs, Phys. Rev. Lett. **76**, 4773 (1996); J. B. Pendry, A. J. Holden, D. J. Robbins, and W. J. Stewart, J. Phys.: Condens. Matter **10**, 4785 (1998); J. B. Pendry, A. J. Holden, D. J. Robbins, and W. J. Stewart, IEEE Trans. Microwave Theory Tech. **47**, 2075 (1999).

[9] R. A. Shelby, D. R. Smith, and S. Schultz, Science **292**, 77 (2001).

[10] A. N. Lagarkov and V. N. Kissel, Phys. Rev. Lett. **92**, 077401 (2004).

[11] I. V. Shadrivov, A. A. Sukhorukov, and Y. S. Kivshar, Phys. Rev. E **67**, 057602 (2003).

[12] S. A. Ramakrishna, J. B. Pendry, D. Schurig, D. R. Smith, and S. Schultz, J. Mod. Opt. **49**, 1747 (2002); B.-I. Wu, T. M. Grzegorczyk, Y. Zhang, and J. A. Kong, J. Appl. Phys. **93**, 9386 (2003); Y. He, Z. Cao, Q. Shen, Opt. Commun. **245**, 125 (2005).

[13] D.-K. Qing and G. Chen, Appl. Phys. Lett. **84**, 669 (2004).

[14] We include the term "plasmon" in the naming of the investigated surface polaritons, to denote that the dielectric constant $\varepsilon(\omega)$ and the magnetic permeability $\mu(\omega)$ of the LH material are described macroscopically by a plasma dispersion law, as explained in Ref. 9.

[15] B. Prade, J. Y. Vinet, and A. Mysyrowicz, Phys. Rev. B **44**, 13556 (1991).

[16] J. J. Burke, G. I. Stegeman, and T. Tamir, Phys. Rev. B **33**, 5186 (1986).

[17] I. V. Shadrivov, A. A. Sukhorukov, Y. S. Kivshar, A. A. Zharov, A. D. Boardman, and P. Egan, Phys. Rev. E **69**, 016617 (2004).

[18] R. A. Shelby, D. R. Smith, S. C. Nemat Nasser, and S. Shultz, Appl. Phys. Lett. **78**, 489 (2001).

[19] A. Snyder and J. D. Love, *Optical Waveguide Theory* (Chapman and Hall, New York, 1983).

[20] H. Kogelnic and V. Ramaswamy, Appl. Opt. **13**, 1857 (1974).

[21] R. Loudon, J. Phys. A **3**, 233 (1970); R. Ruppin, Phys. Lett. A **299**, 309 (2002).

[22] M. F. Yanik and S. Fan, Phys. Rev. Lett. **92**, 083901 (2004).